A FULLY UNSUPERVISED HYPERSPECTRAL UNMIXING ALGORITHM DEALING WITH NONLINEARITY AND SPECTRAL VARIABILITY FOR COMPLEX REAL-WORLD SCENES

Fatima Zohra Benhalouche [1, 2], *Moussa Sofiane Karoui* [1, 2] and *Yannick Deville* [2]

[1] Agence Spatiale Algérienne, Centre des Techniques Spatiales, Arzew, Algeria
[2] Univ Toulouse, CNES, CNRS, IRAP, Toulouse, France

ABSTRACT

The analysis of complex real-world scenes, such as urban environments, through hyperspectral remote sensing imaging, provides a wealth of valuable data for characterizing materials and physical phenomena present within such observed scenes. However, the exploitation of these data often faces major constraints related to the specific nature of these environments, such as the complexity of their spectral mixing models combined with the low spatial resolution of spaceborne hyperspectral sensors providing these data to be processed. Indeed, landscape heterogeneity and topography induce non-linear interactions, such as multiple light reflections, combined with significant spectral variability caused by material diversity and atmospheric conditions. This study proposes a fully unsupervised hyperspectral unmixing algorithm, based on nonnegative matrix factorization, which jointly addresses nonlinearity and spectral variability. The performance of the proposed algorithm is evaluated through experiments conducted on real hyperspectral data, acquired over an urban area, to demonstrate its effectiveness in improving the processing of data of real-world scenes.

Index Terms— Hyperspectral data, hyperspectral unmixing, nonlinear mixing model, spectral variability phenomenon, nonnegative matrix factorization.

1. INTRODUCTION

Compared to rural or natural areas, complex environments, such as urban areas, are distinguished by specific spectral characteristics, which are directly influenced by the physicochemical properties of materials present in these scenes and the complex light interactions occurring in such environments [1], [2].

In this context, hyperspectral remote sensing imagery, thanks to its ability to capture data in hundreds of narrow and contiguous spectral bands, constitutes a privileged analysis tool that enables a fine characterization of complex environment dynamics [3]. This is fundamental for a wide range of applications, from urban planning to climate and environmental monitoring [1]. However, the exploitation of this technology in urban environments remains constrained by technological limitations of hyperspectral sensors and the structural complexity of such environments [4].

Indeed, the low spatial resolution of, in particular, spaceborne hyperspectral sensors results in mixed spectra that combine more than one pure material spectra (called endmembers). This prevents direct identification of such endmembers and requires additional processing to separate these mixed spectra [4].

In its most basic form, this combination is modeled as a linear mixture of pure material spectra, where each of the latter spectra is weighted by its abundance fraction, thus representing the proportion of appearance of each pure material present in each observed pixel [4].

However, data coming from real-world scenes often involve more complex mixing phenomena, in particular, in the presence of a significant non-flat landscape and/or irradiance heterogeneity. In such configurations, the mixing model becomes intrinsically nonlinear, making data analysis more difficult [5]–[7].

Another major challenge faced in real-world scenes is the "spectral/intra-class variability" phenomenon [8]–[11]. This phenomenon appears as fluctuations within spectral signatures of the same class of material within an observed scene. These variations result from multiple factors, including the intrinsic diversity of materials present in an imaged scene, variations in lighting and atmospheric conditions, spatial variations, or material composition [8].

Therefore, to guarantee accurate analysis of such hyperspectral data, it is essential to take into account both mixture nonlinearity and spectral variability. To address these issues, hyperspectral unmixing approaches are the main techniques considered for carrying out the process of decomposing the mixed pixel spectra of observed hyperspectral data into their constituent pure material spectra and their corresponding abundance fractions, in accordance with a pre-established mixing model [4].

In this study, a fully unsupervised algorithm, which jointly addresses mixture nonlinearity and spectral variability, is proposed. The two issues are usually treated separately, which limits the accuracy of analyses in urban or heterogeneous contexts. This contribution uses a recently designed data mixing model [12], which considers nonlinearity and spectral variability, and proposes an associated fully unsupervised unmixing algorithm based on the mathematical optimization framework of Nonnegative Matrix Factorization (NMF) [13].

The proposed fully unsupervised algorithm has the following two specific features. First, it is based on previous bilinear/linear-quadratic mixing models known for their ability to model multiple light reflections. Second, whereas conventional algorithms assume a unique spectrum for each material, the designed algorithm overcomes this limitation by integrating spectral variability directly into the factorization process, allowing the distinction between variations due to physical interactions (i.e., nonlinearity) and those induced by intrinsic changes in materials or acquisition conditions (i.e., spectral/intra-class variability). By jointly managing these two phenomena, the designed algorithm allows a more accurate estimation of abundance fractions and a more precise

identification of materials, even in scenes marked by pronounced relief or changing atmospheric conditions. Indeed, this synergy between physical modeling and statistical flexibility makes it possible to process more effectively a wider range of real-world scenes observed in Earth observation works.

Furthermore, most importantly, this study extends the work introduced in [12], but whereas this previous work used predefined and fixed (i.e., without update during the optimization process) spectra, the current designed algorithm is completely unsupervised: spectra are now updated and estimated iteratively during the proposed optimization framework. This is achieved after a more suitable rewriting of the considered cost function in order to more easily deduce an NMF-based rule for iteratively updating the spectra. The designed algorithm offers increased flexibility, allowing for dynamic unsupervised adaptation to the specific characteristics of the data being processed.

The remainder of this paper is organized as follows. Section 2 describes the considered data mixing model, whereas Section 3 introduces the corresponding fully unsupervised hyperspectral unmixing algorithm. Experimental results are detailed in Section 4, and Section 5 concludes this investigation.

2. CONSIDERED DATA MIXING MODEL

As a reminder, the data model considered in this work is described below. In this model, each spectral vector associated with a pixel in a hyperspectral image is defined as follows [5], [12]

$$x_i = \sum_{j=1}^{M} r_{i,j} c_j(i) + \sum_{j=1}^{M} \sum_{k=j}^{M} (r_{i,j} \odot r_{i,k}) c_{(j,k)}(i), \quad \text{with} \begin{cases} c_j(i) \geq 0, & j = 1 \dots M \\ \sum_{j=1}^{M} c_j(i) = 1, & i = 1 \dots P \\ 0 \leq c_{(j,k)}(i) \leq 0.5, & 1 \leq j \leq k \leq M \end{cases}, \tag{1}$$

where the operator $\odot$ denotes the element-wise multiplication. The vector $r_{i,j} \in \mathbb{R}_+^{L \times 1} \leq 1$ represents the nonnegative reflectance spectrum associated with the j^{th} class of materials and pixel i.

The product $r_{i,j} \odot r_{i,k}$ is here considered as a nonnegative "pseudo-endmember" spectrum. The coefficients $c_j(i)$ and $c_{(j,k)}(i)$ respectively correspond to the nonnegative linear and quadratic abundances of pure material(s) j or j and k in pixel i, with $c_j(i)$ satisfying the abundance sum-to-one constraint. Finally, M and P denote the number of endmembers and pixels, respectively, and L denotes the number of spectral bands.

To address the spectral variability phenomenon, the model of $r_{i,j}$ is defined by [10]

$$r_{i,j} = a_{i,j} \odot e_{Ref_j}, \tag{2}$$

where $a_{i,j} \in \mathbb{R}_+^{L \times 1}$ denotes the vector of nonnegative variability coefficients for the version of the j^{th} class of endmembers associated with pixel i, and $e_{Ref_j} \in \mathbb{R}_+^{L \times 1}$ is the pixel-independent nonnegative reference reflectance spectrum, associated with the j^{th} class.

Introducing this model in Equation (1) gives the considered data mixing model.

$$x_i = \sum_{j=1}^{M} (a_{i,j} \odot e_{Ref_j}) c_j(i) + \sum_{j=1}^{M} \sum_{k=j}^{M} (a_{i,j} \odot e_{Ref_j}) \odot (a_{i,k} \odot e_{Ref_k}) c_{(j,k)}(i), \tag{3}$$

which can be rewritten as follows

$$x_i = \sum_{j=1}^{M} (a_{i,j} \odot e_{Ref_j}) c_j(i) + \sum_{j=1}^{M} \sum_{k=j}^{M} a_{i,(j,k)} \odot (e_{Ref_j} \odot e_{Ref_k}) c_{(j,k)}(i), \quad \text{with } a_{i,(j,k)} = a_{i,j} \odot a_{i,k}. \tag{4}$$

The scale coefficient vectors $a_{i,j}$ adjust the spectra $r_{i,j}$ relative to the reference spectra e_{Ref_j} and are subject to the following constraints.

$$0^{L \times 1} < \alpha^{L \times 1} \leq a_{i,j} \leq \beta^{L \times 1}, \tag{5}$$

where $\alpha^{L \times 1}$ and $\beta^{L \times 1}$ are fixed coefficient vectors defining the minimum and maximum variability levels. For all pixels, the resulting mixing model can be compactly expressed in matrix form as

$$X = \left(A \odot (E_{Ref} \mathbb{1}^{1 \times P} \otimes Id_N)\right) C, \tag{6}$$

where $X \in \mathbb{R}_+^{L \times P}$ is the observed data matrix, $\mathbb{1}^{1 \times P} \in \mathbb{R}_+^{1 \times P}$ is a unit row vector, and $Id_N \in \mathbb{R}_+^{N \times N}$ is the identity matrix. The operator $\otimes$ is the Kronecker multiplication operator, with $N = 2 \times M + \frac{M(M-1)}{2}$ the number of endmembers and pseudo-endmember.

The matrix $A \in \mathbb{R}_+^{L \times (NP)}$ holds all nonnegative variability coefficients and can be written as

$$A = [A_1 | A_2 | \quad \cdots \quad | A_P], \quad \text{with } A_t \in \mathbb{R}_+^{L \times N} \ (t = 1 \dots P), \text{ and } A_i = [A_{t_{lin}} A_{t_{qua}}], \tag{7}$$

where $A_{t_{lin}} = [a_{t,1} \dots a_{t,M}]$ and $A_{t_{qua}} = [a_{t,1} \odot a_{t,1}, a_{t,1} \odot a_{t,2} \dots a_{t,M} \odot a_{t,M}]$ with $a_{t,j} \in \mathbb{R}_+^{L \times 1}$.

The matrix $E_{Ref} \in \mathbb{R}_+^{L \times N}$ holds the N-endmember and pseudo-endmember reference spectra. Finally, $C \in \mathbb{R}_+^{(NP) \times P}$ is a block-diagonal matrix of linear and quadratic abundance fractions, corresponding to the transpose of the matrix defined in [9].

3. DESIGNED FULLY UNSUPERVISED NMF-BASED HYPERSPECTRAL UNMIXING ALGORITHM

The proposed fully unsupervised unmixing algorithm relies on a pixel-by-pixel NMF approach to model the mixing function defined in Equation (6). It estimates the matrices $\tilde{A}$, $\tilde{E}_{Ref}$ and $\tilde{C}$ that respectively correspond to A, E_{Ref} and C, using multiplicative update rules to minimize the following cost function

$$J = \frac{1}{2}\left\|X - \left(\tilde{A} \odot (\tilde{E}_{Ref} \mathbb{1}^{1\times P} \otimes Id_N)\right)\tilde{C}\right\|_F^2, \quad (8)$$

where $\|.\|_F$ represents the Frobenius norm.

As a reminder, and using the work reported in [12], the iterative and multiplicative update rules of $\tilde{A}$ and $\tilde{C}$ are as follows

$$\tilde{A} \leftarrow \tilde{A} \odot \left(X\tilde{C}^T\right) \oslash \left(\left(\tilde{A} \odot (\tilde{E}_{Ref} \mathbb{1}^{1\times P} \otimes Id_N)\right)\tilde{C}\tilde{C}^T + \varepsilon\right), \quad (9)$$

$$\tilde{C} \leftarrow \tilde{C} \odot \left(\left(\tilde{A} \odot (\tilde{E}_{Ref} \mathbb{1}^{1\times P} \otimes Id_N)\right)^T X\right) \oslash \left(\left(\tilde{A} \odot (\tilde{E}_{Ref} \mathbb{1}^{1\times P} \otimes Id_N)\right)^T \left(\tilde{A} \odot (\tilde{E}_{Ref} \mathbb{1}^{1\times P} \otimes Id_N)\right)\tilde{C} + \varepsilon\right), \quad (10)$$

where $\oslash$ denotes the element-wise division and ε is a very small and positive value added to the denominator of each update rule to avoid division by zero. The matrix $\tilde{A}$ contains linear and quadratic variability coefficients, with quadratic terms constrained by the linear ones as follows [12]

$$\left[\tilde{A}\right]_{l,(1-i)N+M+(j,k)} = \left[\tilde{A}\right]_{l,j(1-i)N+j} \times \left[\tilde{A}\right]_{l,(1-i)N+k}, \quad \text{with} \begin{cases} i = 1 \dots P \\ l = 1 \dots L \\ j = 1 \dots M \\ 1 \le j < k \le M \end{cases}, \quad (11)$$

Furthermore, to ensure physical consistency, the following constraints are considered [12]

$$\tilde{A} \odot \left(\tilde{E}_{Ref} \mathbb{1}^{1\times P} \otimes Id_N\right) \le 1^{L\times(NP)}, \quad (12)$$

$$\alpha^{L\times(NP)} \le \tilde{A} \le \beta^{L\times(NP)}. \quad (13)$$

$$\tilde{A} \leftarrow \max\{\tilde{A}, \alpha^{L\times(MP)}\}, \quad (14)$$

$$\tilde{A} \leftarrow \min\{\tilde{A}, \beta^{L\times(MP)}, 1^{L\times(MP)} \oslash (\tilde{E}_{Ref} \mathbb{1}^{1\times P} \otimes Id_N + \varepsilon)\}. \quad (15)$$

Additional constraints are applied to the abundance matrix $\tilde{C}$ [12]. Linear abundances satisfy the sum-to-one constraint, while linear and quadratic abundances are upper-bounded by, respectively, μ_1 and μ_2. The corresponding operations on the proposed algorithm read as follows

$$\left[\tilde{C}_{(i-1)N+j,i}, \dots, \tilde{C}_{(i-1)N+M,i}\right] = \left[\tilde{C}_{(i-1)N+j,i}, \dots, \tilde{C}_{(i-1)N+M,i}\right] / \sum_{j=1}^{M} \tilde{C}_{(i-1)N+j,i}, \quad (16)$$

$$\tilde{C}_{(i-1)N+M+j,i} = min\left\{\tilde{C}_{(i-1)N+M+j,i}, \mu_1\right\}, \quad (17)$$

$$\tilde{C}_{(i-1)N+2M+(j,p),i} = min\left\{\tilde{C}_{(i-1)N+2M+(j,p),i}, \mu_2\right\}, \quad (18)$$

In this paper, unlike [12], where the matrix E_{Ref} of endmember spectra is assumed to be known and fixed, the main contribution proposed in this work consists of updating also an estimate of that matrix noted $\tilde{E}_{Ref}$, thus making the unmixing algorithm completely and fully unsupervised. Furthermore, since this matrix comprises a linear part (M-endmember reference spectra) and a quadratic part (pseudo-endmember reference spectra) that only depends on the former matrix, the gradient expression of the considered cost function with respect to spectra is calculated only with respect to its linear component.

To facilitate the derivation of the gradient expression of the considered cost function J with respect to spectra, this one is rewritten as follows

$$J = \frac{1}{2}\sum_{l,i}\left[X - \left(\left(\tilde{A} \odot (\tilde{E}_{Ref} \mathbb{1}^{1\times P} \otimes Id_N)\right)\tilde{C}\right)\right]_{l,i}^2, \quad (19)$$

$$J = \frac{1}{2}\sum_{l,i}\left[X_{l,i} - \sum_{j=1}^{M}\left(\left(\tilde{A}_{l,v} \odot \left(\tilde{E}_{Ref}{}_{l,j} \mathbb{1}^{1\times P} \otimes Id_M\right)\right)\tilde{C}_{v,i}\right) - \sum_{j=1}^{M}\sum_{k=1}^{M}\left(\left(\tilde{A}_{l,w} \odot \left((\tilde{E}_{Ref}{}_{l,j} \times \tilde{E}_{Ref}{}_{l,k})\mathbb{1}^{1\times P} \otimes Id_{N-M}\right)\right)\tilde{C}_{w,i}\right)\right]^2, \quad \text{with} \begin{cases} v = (1-i)N + j & i = 1 \dots P \\ w = (1-i)N + M + (j,k) & j = 1 \dots M \\ 1 \le j < k \le M & l = 1 \dots L \end{cases} \quad (20)$$

Using Equation (20), the gradient expression of J, with respect to an element $\tilde{E}_{Ref}{}_{l,k}$ of the linear part of the matrix $\tilde{E}_{Ref}$, can be expressed as follows

$$\frac{\partial J}{\partial \tilde{E}_{Ref}{}_{l,k}} = -\sum_{i=1}^{P}\left[\left(X\tilde{C}^T - \left(\left(\tilde{A} \odot \left(\tilde{E}_{Ref} \mathbb{1}^{1\times P} \otimes Id_N\right)\right)\tilde{C}\right)\tilde{C}^T\right) \odot \tilde{A}\right]_{l,(i-1)N+k} - \sum_{j=1,k=1}^{M}\left(1 + \delta_j^k\right) \times \left[\tilde{E}_{Ref}\right]_{l,j} \times \left[\left(X\tilde{C}^T - \left(\left(\tilde{A} \odot \left(\tilde{E}_{Ref} \mathbb{1}^{1\times P} \otimes Id_N\right)\right)\tilde{C}\right)\tilde{C}^T\right) \odot \tilde{A}\right]_{l,(i-1)N+M+(j,k)}, \quad \text{with} \begin{cases} \delta_j^k = 0 & if\ k \ne j \\ \delta_j^k = 1 & if\ k = j \end{cases} \quad (21)$$

Moreover, two matrix variables V and W are introduced

$$V = \left(X\tilde{C}^T\right) \odot \tilde{A}, \quad (22)$$

$$W = \left(\left(\left(\tilde{A} \odot (\tilde{E}_{Ref} \mathbb{1}^{1\times P} \otimes Id_N)\right)\tilde{C}\right)\tilde{C}^T\right) \odot \tilde{A}. \quad (23)$$

Thus, the update rule of an element of the linear part of the endmember spectra $\tilde{E}_{Ref}$ is

$$\tilde{E}_{Ref}{}_{l,k} \leftarrow \tilde{E}_{Ref}{}_{l,k} \times \frac{\sum_{i=1}^{P}[V]_{l,(i-1)N+k} + \sum_{j=1,k=1}^{M}\left(1+\delta_j^k\right) \times \left[\tilde{E}_{Ref}\right]_{l,j} \times [V]_{l,(i-1)N+M+(j,k)}}{\sum_{i=1}^{P}[W]_{l,(i-1)N+k} + \sum_{j=1,k=1}^{M}\left(1+\delta_j^k\right) \times \left[\tilde{E}_{Ref}\right]_{l,j} \times [W]_{l,(i-1)N+M+(j,k)} + \varepsilon}, \quad \text{with } \tilde{E}_{Ref}{}_{l,k} = max\left\{\tilde{E}_{Ref}{}_{l,k}, 0\right\}, \quad (24)$$

The update rule of an element of the quadratic part of the spectra matrix $\tilde{E}_{Ref}$ is

$$\left[\tilde{E}_{Ref}\right]_{l,(j,k)} = \left[\tilde{E}_{Ref}\right]_{l,j} \times \left[\tilde{E}_{Ref}\right]_{l,k}, \quad (25)$$

In the designed fully unsupervised hyperspectral unmixing algorithm, the initial values of the key matrix variables are

carefully selected. First, each spectral variability coefficient is assigned a fixed value equal to one. In addition, the spectra contained in $\tilde{E}_{Ref}$ are initialized using the Vertex Component Analysis (VCA) method [4]. Furthermore, each non-zero initial value of the abundance coefficients matrix $\tilde{C}$ is set to $1/M$.

Finally, to control the computational cost while ensuring adequate convergence of the algorithm, a predefined maximum number of iterations is adopted as a stopping criterion for the proposed algorithm.

4. EXPERIMENTAL RESULTS

4.1. Tested data

In this study, the tested data consists of a real, radiometrically and geometrically corrected, hyperspectral data covering a part of the North-Eastern urban area of Oran, Algeria. The data were acquired by the PRISMA sensor on September 7, 2024, with a spatial resolution of 30 m and 234 spectral bands spanning the VNIR and SWIR spectral regions. For analysis, only 103 bands are kept, while the remaining bands are discarded due to noise and atmospheric absorption.



Figure 1. True-color image composite of the tested real data.

4.2. Performance evaluation criteria

To assess the performance of the tested algorithms, some quantitative criteria are considered. They include the reconstruction Spectral Angle Mapper (rSAM), the reconstruction Root Mean Square Error (rRMSE) and the Reconstruction Error (RE), computed between the original and the reconstructed hyperspectral images.

4.3. Obtained results

The results obtained with the designed fully unsupervised algorithm are compared with those of tested NMF-based unmixing approaches: the supervised one addressing spectral variability and nonlinearity [12] (without updating the spectra), a second approach dealing only with spectral variability [10], and finally a third one that addresses only nonlinearity [14].

These tested algorithms are initialized using identical values for the corresponding model parameters and matrices. Furthermore, all coefficients of the matrix $\alpha^{L\times(MP)}$(respectively $\beta^{L\times(MP)}$), as defined in (13) and controlling the minimum (respectively maximum) degree of spectral variability, are equal to 0.8 (respectively 1.2).

The reported results correspond to averages obtained over ten different initializations. Table I summarizes the values achieved by the considered performance metrics.

Table I. Mean values of the evaluation criteria for the tested hyperspectral data.

	Proposed algorithm	[12]	[10]	[14]
rSAM(°)	**0.6909**	1.1721	4.4779	5.2883
rRMSE	**0.0064**	0.0102	0.0653	0.0642
RE	**0.0004**	0.0018	0.0956	0.0801

Figures 2 and 3 show, respectively, the $rSAM$ and the $rRMSE$ criteria maps calculated between the original data and the reconstructed ones.

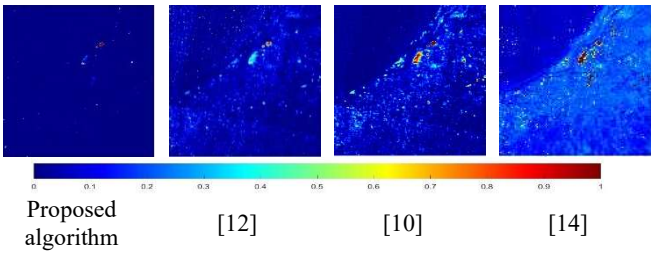


Figure 2. $rSAM$ maps obtained between the original image and the reconstructed one.

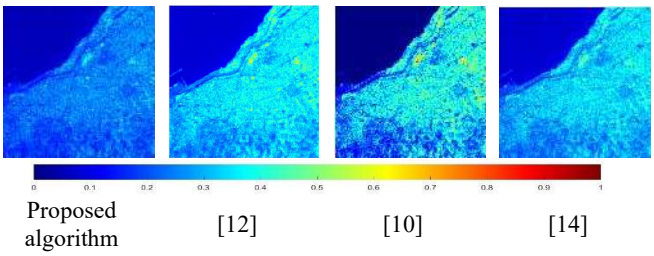


Figure 3. $rRMSE$ maps obtained between the original image and the reconstructed one.

The obtained results show that the proposed algorithm achieves the best performance for all evaluation metrics, with the lowest $rSAM$, $rRMSE$, and RE values. This indicates superior spectral preservation and minimal reconstruction error compared to the tested literature methods, confirming the effectiveness of the proposed algorithm for hyperspectral data processing.

5. CONCLUSION

In this paper, a fully unsupervised hyperspectral unmixing algorithm based on nonnegative matrix factorization is designed. The proposed unsupervised method jointly accounts for nonlinearity and spectral variability. It relies on a nonlinear data mixing model designed to effectively model and address nonlinear interactions and spectral variations inherent in hyperspectral data.

Experimental results demonstrate that the proposed unsupervised unmixing algorithm achieves promising performance for the analysis of hyperspectral data acquired from complex real-world scenes, while explicitly accounting for spectral variability within the considered nonlinear mixing model.

6. REFERENCES

[1] C. Weber, X. Briottet, T. Houet, S. Gadal, R. Aguejdad, Y. Deville, M. Dalla-Mura, C. Mallet, A. Le Bris, M.S. Karoui, F.Z. Benhalouche, K. Djerriri, S. Fabre, and J. Aval, "Hyperspectral Imagery and Urban Areas: Results of The HYEP Project," *Revue Française de Photogrammétrie et de Télédétection*, vol. 224(1), pp. 75–92, December 2022, doi: 10.52638/rfpt.2022.589.

[2] D. Yu and C. Fang, "Urban Remote Sensing with Spatial Big Data: A Review and Renewed Perspective of Urban Studies in Recent Decades," *Remote Sensing*, vol. 15(5), p. 1307, February 2023, doi: 10.3390/rs15051307.

[3] C. Weber, R. Aguejdad, X. Briottet, J. Avala, S. Fabre, J. Demuynck, E. Zenou, Y. Deville, M.S. Karoui, F.Z. Benhalouche, S. Gadal, W. Ourghemmi, C. Mallet, A. Le Bris, and N. Chehata, "Hyperspectral Imagery for Environmental Urban Planning," *In Proceedings of the IGARSS 2018—2018 IEEE International Geoscience and Remote Sensing Symposium*, Valencia, Spain, 22–27 July 2018, pp. 1628–1631. doi: 10.1109/IGARSS.2018.8519085.

[4] J.M. Bioucas-Dias, A. Plaza, N. Dobigeon, M. Parente, Q. Du, P. Gader, and J. Chanussot, "Hyperspectral Unmixing Overview: Geometrical, Statistical, and Sparse Regression-Based Approaches," I*EEE Journal of Selected Topics in Applied Earth Observations and Remote Sensing*, vol. 5(2), pp. 354-379, 2012. doi: 10.1109/JSTARS.2012.2194696.

[5] I. Meganem, P. Deliot, X. Briottet, Y. Deville, and S. Hosseini, "Linear–Quadratic Mixing Model for Reflectances in Urban Environments," *IEEE Transactions on Geoscience and Remote Sensing*, vol. 52(1), Art. no. 1, January 2014, doi: 10.1109/TGRS.2013.2242475.

[6] N. Dobigeon, Y. Altmann, N. Brun, and S. Moussaoui, "Linear and Nonlinear Unmixing in Hyperspectral Imaging," *In Data Handling in Science and Technology*, vol. 30, Elsevier, 2016, pp. 185–224. doi: 10.1016/B978-0-444-63638-6.00006-1.

[7] R. Heylen and P. Scheunders, "A Multilinear Mixing Model for Nonlinear Spectral Unmixing," *IEEE Transactions on Geoscience and Remote Sensing*, vol. 54(1), Art. no. 1, January 2016, doi: 10.1109/TGRS.2015.2453915.

[8] A. Zare and K.C. Ho, "Endmember variability in hyperspectral analysis: Addressing spectral variability during spectral unmixing," *IEEE Signal Processing Magazine*, vol. 31(1), pp. 95-104, 2014. doi: 10.1109/MSP.2013.2279177.

[9] C. Revel, Y. Deville, V. Achard, X. Briottet, and C. Weber, "Inertia-constrained pixel-by-pixel nonnegative matrix factorization: a hyperspectral unmixing method dealing with intra-class variability," *Remote Sensing*, vol. 10(11), 1706, 2018. https://doi.org/10.3390/rs10111706.

[10] F.Z. Benhalouche, M.S. Karoui, and Y. Deville, "An NMF-Based Approach for Hyperspectral Unmixing Using a New Multiplicative-tuning Linear Mixing Model to Address Spectral Variability," *In 2019 27th European Signal Processing Conference* (*EUSIPCO*), A Coruna, Spain, September 2019, pp. 1–5. doi: 10.23919/EUSIPCO.2019.8902707.

[11] Y. Deville, G. Faury, V. Achard, X. Briottet, "An NMF-based method for jointly handling mixture nonlinearity and intraclass variability in hyperspectral blind source separation", Digital Signal Processing, vol. 133, March 2023, paper no. 103838. DOI: https://doi.org/10.1016/j.dsp.2022.103838.

[12] F.Z. Benhalouche, M.S. Karoui, and Y. Deville, "A Novel Hyperspectral Unmixing Approach Jointly Addressing Nonlinearity and Spectral Variability in Urban Environments," *In Proceedings of the IGARSS 2025—2025 IEEE International Geoscience and Remote Sensing Symposium*, Brisbane, Australia, 3–8 August 2025, pp. 8738–8742. doi: 10.1109/IGARSS55030.2025.11243933.

[13] A. Cichocki, R. Zdunek, A. H. Phan, and S. Amari, *Nonnegative matrix and tensor factorizations: Applications to exploratory multi-way data analysis and blind source separation*. John Wiley and Sons, 2009.

[14] I. Meganem, Y. Deville, S. Hosseini, P. Deliot, and X. Briottet, "Linear-Quadratic Blind Source Separation Using NMF to Unmix Urban Hyperspectral Images," *IEEE Transactions on Signal Processing*, vol. 62(7), Art. no. 7, April 2014, doi: 10.1109/TSP.2014.2306181.